ISSN 1808-8546 (ONLINE) 1808-3765 (CD-ROM)

ANÁLISE DE CANAVIAIS IRRIGADOS COM PARÂMETROS BIOFÍSICOS POR SENSORIAMENTO REMOTO NO NORDESTE BRASILEIRO

JADIENE MOURA DOS SANTOS [1*]; PABRÍCIO MARCOS OLIVEIRA LOPES[2]; GEBER BARBOSA DE ALBUQUERQUE MOURA[3]; ANDERSON SANTOS DA SILVA[4]; JHON LENNON BEZERRA DA SILVA[5], JOSÉ GALDINO DE OLIVEIRA JÚNIOR[6]

[*] *Esta pesquisa refere-se ao trabalho de iniciação científica da primeira autora.*
[1] *Engenheira Florestal, Universidade Federal Rural de Pernambuco, Rua Dom Manuel de Medeiros, s/n, Dois Irmãos, Recife/PE. E-mail: mourajad@hotmail.com;*
[2] *Professor Dr. da Universidade Federal Rural de Pernambuco, Rua Dom Manuel de Medeiros, s/n, Dois Irmãos, Recife/PE. E-mail: pabricio.lopes@ufrpe.br;*
[3] *Professor Dr. da Universidade Federal Rural de Pernambuco, Rua Dom Manuel de Medeiros, s/n, Dois Irmãos, Recife/PE. E-mail:geber.moura@ufrpe.br;*
[4] *Professor Dr. da Universidade Federal do Agreste de Pernambuco, Avenida Bom Pastor, s/n, Boa Vista, Garanhuns/PE. E-mail: anderson.silva@ufape.edu.br;*
[5] *Doutor em Engenharia Agrícola, Universidade Federal Rural de Pernambuco, Rua Dom Manuel de Medeiros, s/n, Dois Irmãos, Recife/PE. E-mail: jhonlennoigt@hotmail.com;*
[6] *Mestrando em Engenharia Agrícola, Universidade Federal Rural de Pernambuco, Rua Dom Manuel de Medeiros, s/n, Dois Irmãos, Recife/PE: dinojr95@gmail.com.*

1 RESUMO

A cultura da cana-de-açúcar ocupa uma área significativa no município de Juazeiro, BA, afetando o ambiente em que está inserida. O uso de tecnologias como as técnicas de sensoriamento remoto e geoprocessamento, vem auxiliando na obtenção de informações importantes sobre essas áreas agrícolas. O objetivo deste trabalho foi avaliar a distribuição espacial dos componentes do balanço de radiação à superfície em áreas agrícolas com o cultivo de cana-de-açúcar irrigado no semiárido brasileiro. O estudo foi realizado em uma porção da região do Vale do Submédio do São Francisco, especificadamente em uma área comercial cultivada com cana-de-açúcar totalmente irrigada, localizada no município de Juazeiro, BA. Foram obtidos por meio de sensoriamento remoto, os parâmetros biofísicos (NDVI, temperatura da superfície, albedo da superfície e saldo de radiação) e a classificação supervisionada Máxima Verossimilhança (Maxver) para as datas 03/09/2013, 22/09/2014 e 24/08/2015 a partir do processamento digital de imagens do satélite Landsat-8, utilizando o software QGIS. Através da Maxver foi possível detectar os diferentes estágios fenológicos (inicial e de maturação) dos cultivos de cana-de-açúcar presentes na região; além disso, os resultados demostraram que os valores de NDVI são inversamente proporcionais aos de temperatura. Os altos valores de albedo e baixos de Rn estão relacionados à existência de solo desnudo e/ou palha de cana-de-açúcar. Por outro lado, o NDVI apresentou-se alto, Ts relativamente baixa, albedo e Rn relativamente moderados na vegetação sadia. A análise espaço-temporal do NDVI e Ts indicou variações na cobertura do solo, destacando a existência de fases distintas de desenvolvimento da cultura em campo. Por fim, a metodologia apresentou-se viável para o mapeamento de variáveis biofísicas nas diferentes datas analisadas.

Palavras-chave: Landsat-8, semiárido, saldo de radiação.

Recebido em 25/01/2021 e aprovado para publicação em 03/11/2021
DOI: http://dx.doi.org/10.15809/irriga.2021v26n3p638-663

SANTOS, J. M.; LOPES, P. M. O.; MOURA, G. B. A.; SILVA, A. S.; SILVA, J. L. B.; OLIVEIRA JÚNIOR, J. G.

ANALYSIS OF IRRIGATED SUGARCANE FIELDS WITH BIOPHYSICAL PARAMETERS BY REMOTE SENSING IN THE BRAZILIAN NORTHEAST

2 ABSTRACT

The cultivation of sugarcane occupies a significant area in the municipality of Juazeiro, BA, affecting the surrounding environment. The use of technologies, such as remote sensing and geoprocessing, has been helping to obtain important information about these agricultural areas. This work aimed to evaluate the spatial distribution of the components of the surface radiation balance in agricultural areas with the cultivation of irrigated sugarcane in the Brazilian semiarid region. This research was carried out in a portion of the Sub-Middle of São Francisco Valley, specifically in a commercial area cultivated with totally irrigated sugarcane, located in the municipality of Juazeiro, BA. The biophysical parameters (NDVI, surface temperature, surface albedo, and radiation balance) and the supervised classification Maximum Likelihood (Maxver) for the dates 09/03/2013, 09/22/2014, and 08/24/2015 were obtained through remote sensing from the digital processing of Landsat-8 satellite images, using the QGIS software. Through Maxver, it was possible to detect the different phenological stages (initial and maturation) of the sugarcane cultivations present in the region. Also, the results showed that the NDVI values are inversely proportional to temperature. The high albedo and low Rn values are related to bare soil and sugarcane straw. However, NDVI was high, Ts relatively low, and albedo and Rn relatively moderate in healthy vegetation. The spatial-temporal analysis of NDVI and Ts indicated variations in soil cover, highlighting distinct phases of development of the crop in the field. Finally, the methodology proved to be viable for mapping biophysical variables on different dates analyzed.

Keywords: Landsat-8, semiarid, radiation balance.

3 INTRODUCTION

Brazil is privileged owing to its climatic conditions for large-scale sugarcane cultivation in all regions of the country, which makes this one of the most important crops in Brazilian agribusiness, with a high production capacity of biomass and derivatives (straw, sugar, alcohol, bagasse, vinasse and energy), which, linked to incentives from the Federal Government or the consumer market, always remains the focus of investments and technological advances (SILVA *et al*., 2019b).

In the Southeast Region of the country, the states of São Paulo and Minas Gerais stand out as the main sugarcane producers, with the 2019/2020 harvest reaching 436.4 million tons (a 5.2% increase over the previous harvest). The Northeast Region, despite the growth of crops such as soybeans and corn, presented a 0.8% increase in planted area and a 2.8% increase in average productivity, reaching a production of approximately 51 million tons for the 2020/21 harvest (CONAB, 2020).

The state of Bahia has a forecast planted area for the 2020/21 harvest of 61.8 thousand hectares, aiming for an average productivity of close to 59.79 t ha $^{-1}$, which may vary between fully irrigated crops and

those with rescue irrigation, that is, dependent on rainfall at a certain stage of the crop's phenological stage (CONAB, 2020).

Specifically, in the Submédio São Francisco Valley region, even in the midst of a semiarid climate, the municipalities of Petrolina, Pernambuco, and Juazeiro, Bahia, stand out as major hubs for irrigated fruit farming. In Juazeiro, Bahia, sugarcane has been produced over large areas, and sugarcane production can be affected by climate variations. Because it is a monoculture that occupies vast areas and affects the environment in which it is inserted in different ways, it is necessary to evaluate the effects caused by this interaction of the soil–water-plant–atmosphere system (ESTEVES *et al*., 2012; SILVA *et al*., 2019b).

According to the varietal census in Brazil for the 2017/2018 harvest, 66% of the varieties planted belonged to the Interuniversity Network for the Development of the Sugarcane Sector (RIDESA - RB), 14% belonged to the Sugarcane Technology Center (CTC), 13% belonged to Copersucar SA (SP varieties), 2% belonged to the Agronomic Institute of Campinas (IAC), 2% belonged to CanaVialis SA (CV) and 3% were related to other denominations totaling 5.6 million hectares, with the varieties RB867515, RB966928 and RB92579 standing out with 25%, 12% and 10% of the crops, respectively (SILVA, 2019).

With respect to the monitoring and spatiotemporal evaluation of irrigated areas, the use of geoprocessing and remote sensing techniques to obtain biophysical parameters inherent to the energy balance of the Earth's surface are highly viable alternatives, as they are capable of distinguishing the specific spectral response of these targets in terms of land cover and use, especially in terms of the phenological phases of agricultural crops (ANDRADE *et al*., 2014; OLIVEIRA; MORAES; RUDORFF, 2014; SILVA *et al.,* 2015; PAGANI *et al*., 2017; DEBASTIANI *et al.*, 2018; MARTINS *et al*., 2019).

The radiation balance (Rn), or radiation balance, at the soil surface represents the net balance of all the radiant energy received and lost by the surface. This energy is used for nonradiative processes such as evaporation, evapotranspiration, photosynthesis, and heating of the soil and surrounding air, generating turbulent heat exchanges in the atmosphere (VIANELLO; ALVES, 2012). Owing to its importance for sugarcane development, the radiation balance has been the subject of several studies. For example, André *et al.* (2010), analyzing the different stages of sugarcane development, reported that there were no changes in the behavior of the radiation balance, although the absolute values of the terms were different. Moreover, Ferreira Junior *et al.* (2015), investigating the yield and efficiency of radiation use and photosynthesis of irrigated sugarcane in Alagoas, concluded that these variables are not influenced by the use of different row spacings (single and combined).

On the other hand, Oliveira *et al.* (2020), who studied the radiation balance and its energy balance components in a sugarcane cultivation area using different soil cover managements and dry and wet periods, reported that the straw layer on the soil provided greater protection, preventing water loss through soil evaporation, which can be explained by the lower partitioning for evapotranspiration. Sun *et al.* (2018) reported that the energy balance varies depending on the soil cover and the time of year. Flux partitioning is significantly affected by the presence of photosynthetically active vegetation below the soil, while dead vegetation generally has a high albedo value, which causes a decrease in the radiation balance values.

Carvalho, Moura, and Silva (2018), evaluating the changes in radiation balance

caused by the replacement of Caatinga by irrigated sugarcane cultivation areas, reported a 42% increase in surface reflectance when the preserved Caatinga was replaced by sugarcane. Land use change causes significant changes in surface biophysical attributes, altering roughness and aerodynamic properties and, consequently, the energy and mass fluxes of agricultural crops (VON RANDOW *et al*., 2004; LOPES *et al*., 2013; FAUSTO *et al*., 2016; FERNANDES *et al*., 2021a, b).

Thus, several remote sensing (RS) techniques have been used to obtain information related to the Earth's surface and atmosphere through orbital sensors and the implementation of operational algorithms, such as the *surface energy balance algorithm for land* (SEBAL) (BASTIAANSSEN *et al*., 1998a, b).

The SEBAL algorithm is essential in the modeling of geospatial data linked to the surface energy balance at regional and global scales, as it consists of a digital processing method for satellite images that uses semiempirical formulas to obtain biophysical parameters (such as surface albedo, vegetation indices, surface temperature and evapotranspiration) from the spectral channels of the visible, near infrared, and thermal infrared bands and data obtained in the field (BASTIAANSSEN, 2000; BASTIAANSSEN *et al*., 2005; ALVES *et al*., 2017; DEBASTIANI, *et al*., 2018).

On the basis of these computational mathematics procedures, this algorithm has an efficient and validated approach worldwide (TEIXEIRA *et al*., 2009; MATINFAR, 2012; CHÁVEZ *et al*., 2012; TANG *et al*., 2013; ANDRADE *et al*., 2014; MACHADO *et al*., 2014; SILVA *et al*., 2015; ALVES *et al*., 2017; DEBASTIANI, *et al*., 2018). In Brazil, specifically in semiarid regions, some examples of its effectiveness are found in studies on the radiation balance in irrigated areas present in the Caatinga biome (SILVA *et al*., 2012; SILVA *et al*., 2021a).

Surface albedo, through the SEBAL algorithm, becomes a very important biophysical parameter in the study of climate change and environmental impacts, as it is capable of portraying the microclimatic conditions of agricultural crops and radiation absorption, relating them to physical and physiological aspects such as photosynthesis, respiration, radiation balance and evapotranspiration (WANG *et al*., 2001; SILVA; LOPES; AZEVEDO, 2005a; SILVA *et al*., 2020).

The radiation balance, in turn, is a key element in the energy balance, as it is an essential element for understanding the energy exchange processes at the surface/atmosphere interface, mainly in relation to the evapotranspiration process carried out by vegetation and irrigated areas, with applications essentially focused on agricultural meteorology (SILVA; LOPES; AZEVEDO, 2005b; GUSMÃO *et al*., 2012; LOPES *et al*., 2013; OLIVEIRA; SILVA; MOURA, 2015).

Vegetation indices from orbital images are also effective tools for environmental and agricultural monitoring, as they can extract spectral information about vegetation, such as the vigor of its plant biomass. For spectral monitoring of land cover and use, specifically in irrigated areas, the normalized difference vegetation index (NDVI) is worth highlighting *(*HUETE *et al*., 2002; BARBOSA; HUETE; BAETHGEN, 2006; RODRIGUES *et al*., 2020; SILVA; LOPES, 2021). Furthermore, surface temperature (Ts), which is an important indicator of climate change, is essential for monitoring major changes in land use and vegetation due to the severe effects of dry seasons (WENG; QUATTROCHI, 2006; JULIEN; SOBRINO, 2009; SILVA *et al*., 2021b).

Therefore, given the need to analyze large areas and understand the relationships among fundamental variables for the

development of sugarcane fields, the objective was to evaluate, via remote sensing techniques, the spatial distributions of the components of the surface radiation balance in agricultural areas with irrigated sugarcane cultivation in the semiarid region of Brazil.

4 MATERIALS AND METHODS

4.1 Study area

The study was carried out in the Brazilian semiarid region, more specifically, approximately 2,568 ha of the Submiddle São Francisco Valley, which is located between the coordinates of latitude (9°25'14" S and 9°27'57" S) and longitude (40°19'12" W and 40°22'48" W), in the municipality of Juazeiro, BA. This portion belongs to a commercial area cultivated with fully irrigated sugarcane with several varieties of the crop that are adapted to the edaphoclimatic conditions of the region, with cultivar RB92579 standing out as the most commonly used (SÁ, 2016), as illustrated in Figure 1.

Figure 1. Spatial geographic location of the study area.

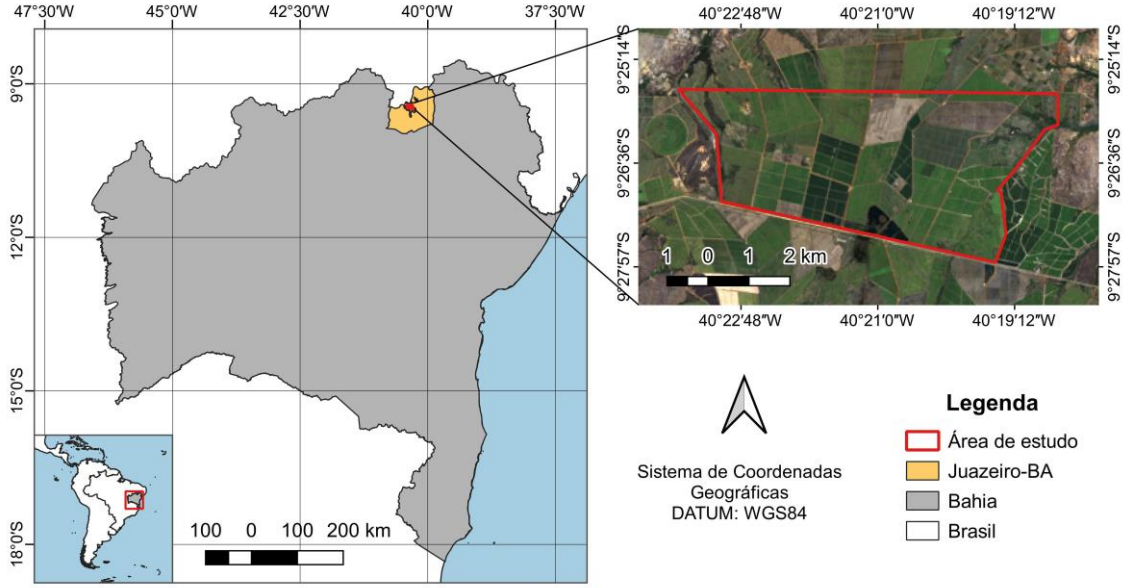

Source: Authors (2021).

The study area has a hot and dry climate due to insufficient annual rainfall, with an average precipitation of 430 mm year $^{-1}$, which is distributed irregularly throughout the year. The average relative humidity is 66%, and the average air temperature is 26.5 °C (PINHEIRO; CRUZ; SIMÕES, 2015; NEMUS, 2016).

The soils of the region were classified as eutrophic solodic planosols, noncalcic brunos, eutrophic cambisols, eutrophic lithic soils and vertisols. In terms of topography, there is flat and undulating relief with open valleys (NASCIMENTO *et al.*, 2012), where the predominant vegetation is the dense shrubby Caatinga, which develops with greater vigor after the first signs of rainfall (CRUZ; BORBA; ABREU, 2005).

Furthermore, four land use types were classified, namely, the early sugarcane stage, development or maturity stage, bare soil stage, and water stage, to facilitate interpretation of the results, as the vegetation cover of the plots presents

different phenological phases. Notably, the sugarcane fields are annual cane.

The RB92579 variety is considered one of the most widely cultivated varieties in sugarcane fields in Brazil. In the Northeast Region, between 2000 and 2015, RB92579 experienced a significant yield increase from 0.5% to 35% of the harvested area, thus demonstrating high agricultural productivity, with an average of 80 t ha $^{-1}$. In some cases, when full irrigation was used, these averages increased from 140 t ha $^{-1}$ to 260 t ha $^{-1}$ over thirteen months of cultivation. This yield potential and its significant presence in sugarcane fields are reflected in its characteristics, which are presented in Table 1.

Table 1. Agricultural and industrial characteristics of the RB92579 variety.

Agricultural and industrial characteristics of the RB 92579 variety	
Area recommendation	Tableland, floodplain, slopes and plain
Tillering in sugarcane plant	High
Tillering in ratoon cane	High
Sprouting of raw ratoon	Good
Sprouting of burnt ratoon	Very good
Closing between lines	Good
Flowering	Eventual
Maturation	Medium to late
Agricultural productivity	High
Environmental requirements	Medium restriction
Resistance to water stress (drought)	Quick recovery
Total Recoverable Sugar (TRS)	High
Long Industrial Period (PUI)	Far away

Source: Interuniversity Network for the Development of the Sugar-Energy Sector - RIDESA (2015).

4.2 Meteorological data

The air temperature (T_a, °C), relative humidity (RH, %), atmospheric pressure (P, hPa), global radiation (RG, W m $^{-2}$), wind speed (ws, ms $^{-1}$), wind direction (Wd, degrees) and rainfall (rain, mm) data were chosen according to the day and time of acquisition of the Landsat-8 satellite images (Table 2). These data belong to the automatic meteorological station of the National Environmental Data Organization (SONDA), which is located in the municipality of Petrolina, PE, at geographic coordinates of 09° 04' 08" S, 40° 19' 11" W and an altitude of 387 m (INPE, 2021).

Table 2. Meteorological data related to the dates of the Landsat 8 satellite images.

Data	DJ	Local Time	T_a (°C)	UR (%)	P (hPa)	RG (W m^{-2})	ws (m s^{-1})	wd (Graus)	Rain (mm)
03/09/2013	246	9h50	26,05	49,19	973,35	803,0	5,14	114,4	0
22/09/2014	265	9h48	31,79	32,71	970,27	849,0	4,76	121,6	0
24/08/2015	236	9h47	26,58	47,62	972,58	809,0	4,16	123,0	0

DJ – Sequential day of the year, Ta – Air temperature, °C – Degrees Celsius, RH – Relative humidity; P – Atmospheric pressure, hPa – Hector Pascal, RG – Global radiation, W m $^{-2}$ – Watt per square meter, ws – Wind speed, ms $^{-1}$ – meter per second, wd – Wind direction.
Source: National Institute for Space Research - INPE (2021)

4.3 Orbital data

The images, which refer to the years 2013--2015, from the *Operational Land Imager (OLI*) and *Thermal Infrared Sensor (TIRS*) sensors, which are located on board the Landsat-8 satellite, were acquired free of charge from the *National Aeronautics and Space Administration* (NASA) website (www.earthexplorer.usgs.gov), considering cloudiness of a maximum of 20% in each orbital scene.

The study area is located in scene 217/67 (orbit/point) in Geotiff format with the original Coordinate Reference System (CRS) WGS 84/UTM Zone 24 N, thus fully covering the analyzed area. Table 3 shows the input data, at the time of the satellite's passage, that were used for the area of interest.

Table 3. Input data at the time of the Landsat-8 satellite passage.

Date	DJ	Time local	Cloud cover (%)	Azimuth Angle (Degrees)	Sun Elevation Angle (Degrees)	Earth-sun distance
09/03/2013	246	09:50	0.01	60.44	58.25	1,008
September 22, 2014	265	09:48	0.00	72.57	62.33	1,003
08/24/2015	236	09:47	0.31	55.92	55.17	1,011

DJ – Sequential day of the year.
Source: United States Geological Survey – USGS (2021).

In the digital preprocessing of the scenes, the steps of clipping, atmospheric correction of reflectances and atmospheric effects (scattering) and reprojection of the geographic coordinate system to the SRC WGS84/UTM zone 24S of the multispectral bands 2, 3, 4, 5, 6, 7 and 10, with a spatial resolution of 30 m, were carried out *via semiautomatic classification plugin* (SCP) tools, which are present in the free *software* QGIS version 2.18.11 (CONGEDO, 2021).

4.4 Digital processing of orbital images

The surface albedo in the shortwave radiation domain (0.3–3.0 μm) without atmospheric correction was obtained through the linear combination of the spectral reflectances of bands 2 to 7 (ρ_λ) obtained from the expression of Silva *et al*. (2016) (Equation 1):

$$\alpha_{Toa} = 0{,}300 \,.\, \rho 2 + 0{,}277 \,.\, \rho 3 + 0{,}233 \,.\, \rho 4 + 0{,}143 \,.\, \rho 5 + 0{,}035 \,.\, \rho 6 + 0{,}012 \,.\, \rho 7 \qquad (1)$$

Then, albedo correction was performed via Equation 2, according to Allen, Tasumi and Trezza (2002):

$$\alpha_{Sup} = (\alpha_{Toa} - \alpha_{atm})/{\tau_{sw}}^2 \quad (2)$$

where α_{atm} is the portion of solar radiation reflected by the atmosphere (0.03) and where τ_{SW} is the atmospheric transmittance, given by Equation 3:

$$\tau_{SW} = 0{,}75 + 2 * 10^{-5} * alt \quad (3)$$

where *alt* is the digital elevation model, represented by an SRTM (*Shuttle Radar Topographic Mission* – Topodata/INPE <http://www.dsr.inpe.br/topodata>) image of the altitude (m) of each pixel.

For calculations of vegetation indices, the normalized difference vegetation index (NDVI), which is sensitive to the quantity and condition of vegetation, was first used. NDVI values range from -1 to +1. Vegetated surfaces have an NDVI between 0 and 1, and water and cloud cover are generally less than zero. The NDVI was calculated according to the equation developed by Rouse *et al*. (1973) (Equation 4). Next, the soil-adjusted vegetation index (SAVI), which assesses vegetative vigor by minimizing soil effects on vegetation, was calculated via the soil adjustment factor (L), as proposed by Huete (1988) (Equation 5). The leaf area index (LAI) is the ratio of the total leaf area of a plant to the area of soil covered by the plant. It is an indicator of canopy biomass and strength. The IAF was calculated via Equation 6, which was developed by Allen, Tasumi and Trezza (2002).

$$NDVI = \frac{\rho IV - \rho V}{\rho IV + \rho V} \quad (4)$$

$$SAVI = \frac{(1+L)(\rho IV - \rho V)}{(L + \rho IV + \rho V)} \quad (5)$$

$$IAF = - (ln ((0{,}69 - SAVI)/0{,}59))/0{,}91 \quad (6)$$

where ρ_{IV} is the reflectance of the near-infrared band; ρ_{V} is the reflectance of the red band; and L is the ground adjustment factor (0.5).

The surface emissivity (ε_0) was calculated on the basis of the leaf area index (LAI) (Equation (6)), as shown in Equation (7) (ALLEN; TASUMI; TREZZA, 2002):

$$\varepsilon 0 = 0{,}95 + 0{,}01 * IAF \quad (7)$$

To calculate the surface temperature (Ts) in Kelvin (K), it is necessary to calculate the brightness temperature (TB) via band 10 of the Landsat-8 TIRS sensor via Equation 8. (https://landsat.usgs.gov/Landsat8_Using_Product.php):

$$TB = K\_2/ln[(K\_1/L\_10) + 1] \quad (8)$$

Therefore, the surface temperature (Ts) was calculated according to Equation 9 (WENG; LU; SCHUBRING, 2004):

$$Ts = TB/((1 + ((\lambda * TB)/c\_2) * ln (\varepsilon o))) \quad (9)$$

where λ is the central wavelength of band 10 equal to 10.895 μm and c_2 is the second radiation constant equal to 14.388 μK.

Then, the longwave radiation emitted by the surface was calculated – Rol ↑ (W m $^{-2}$) for each pixel, using the Stefan–Boltzmann coefficient (σ = 5.67x10 $^{-8}$ W m

$^{-2}$.K $^{-4}$), as a function of T $_s$ and ε $_0$ (Equation 10):

$$Rol \uparrow = \varepsilon 0 * \sigma * Ts^4 \quad (10)$$

The longwave radiation incident on the atmosphere R $_{ol}$ ↓ (W m $^{-2}$) was also calculated via the Stefan–Boltzmann law, described in Equation 10, but as a function of the atmospheric emissivity of the air (ε_a= 0,85* (-ln*τ_{sw})^{0,09}) and T $_a$ (Table 1) in Kelvin (K = T $_a$ + 273.15), according to Equation 11:

$$Rol \downarrow = \varepsilon a * \sigma * Ta^4 \quad (11)$$

To calculate the shortwave radiation incident on the surface, the RS↓ (W m $^{-2}$) Equation (12) was used:

$$RS \downarrow = S * Cos\,\theta * dr * \tau_{SW} \quad (12)$$

where S is the solar constant (1367 W m $^{-2}$) and cos θ is the cos (90° - sun elevation angle).
d $_r$ is the relative Earth–Sun distance, obtained by inverting the square of the Earth–Sun distance found in the image metadata.

Finally, the radiation balance, Rn (W m $^{-2}$), was estimated according to Equation (13):

$$Rn = (1 - \alpha sup)\, RS \downarrow + Rol \downarrow - Rol \uparrow - (1 - \varepsilon o)\, Rol \downarrow \quad (13)$$

4.5 Classification of land use and land cover

The classification of land use and cover was performed via the supervised maximum likelihood (Maxver) classification method, considering the following NDVI stratifications according to Martins *et al*. (2019), described in Table 4.

Table 4. NDVI stratification interval for classifying areas according to their land use and land cover.

Biophysical parameter	Stratification interval	Land use and occupation classes
NDVI	< 0	Water
	0 to 0.199	Bare ground
	0.200 to 0.599	Early stage of development of culture
	>0.600	Crop maturity stage

NDVI – normalized difference vegetation index.
Source: Martins *et al*. (2019).

According to the results of Silva, Bacani and Carvalho (2013), Mulianga et al. (2015) and Cechim, Johann and Antunes (2017), the Maxver model used in this study presents good efficiency in mapping sugarcane areas since, in these works, it was able to provide advanced information on agricultural plantations.

4.6 Statistical analysis

The biophysical parameters obtained throughout the process of estimating the radiation balance were analyzed according to descriptive statistics, and the minimum, maximum and average values calculated in the QGIS computational environment were evaluated.

5 RESULTS AND DISCUSSION

5.1 Analysis based on supervised classification

Figure 2 shows the supervised classification performed to obtain the land use and land cover classes present in the study area, which was commercially cultivated with sugarcane at different times coinciding with the satellite's passage. Various hues related to the phenological stages of the sugarcane analyzed in this study were observed in the different plots, with light green tones indicating an early-stage crop with reduced photosynthetic activity. Furthermore, areas of bare soil (yellow color) and water bodies (blue color) can be identified, thus strengthening the application of land use and land cover classifiers combined with vegetation indices and making them effective tools for monitoring the development stages of agricultural crops in semiarid regions (SILVA *et al*., 2019a).

Figure 2. Qualitative representation of the use and coverage classes of a commercial sugarcane area in Juazeiro, BA, on the dates of 09/03/2013, 09/22/2014 and 08/24/2015.

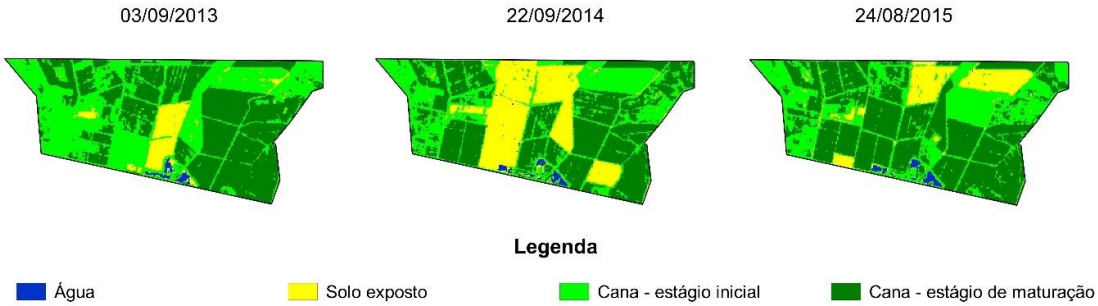

Source: Authors (2021).

On the other hand, Figure 3 shows the areas with the highest photosynthetic activity (Maturation - dark green hue), with percentages of 47.77%, 44.28%, and 53.45% for the years 2013, 2014, and 2015, respectively. The percentage of bare soil also significantly varied between 2013 and 2014, in which the area classified as bare soil significantly increased by 17.39%, demonstrating that crop harvest in the field had already been carried out. However, on August 24, 2015, this same area was still cultivated with sugarcane because of the lower percentage of exposed soil (10.87%).

Figure 3. Quantitative representation of the use and coverage classes of a commercial sugarcane area in Juazeiro, BA, on the dates of 09/03/2013, 09/22/2014 and 08/24/2015.

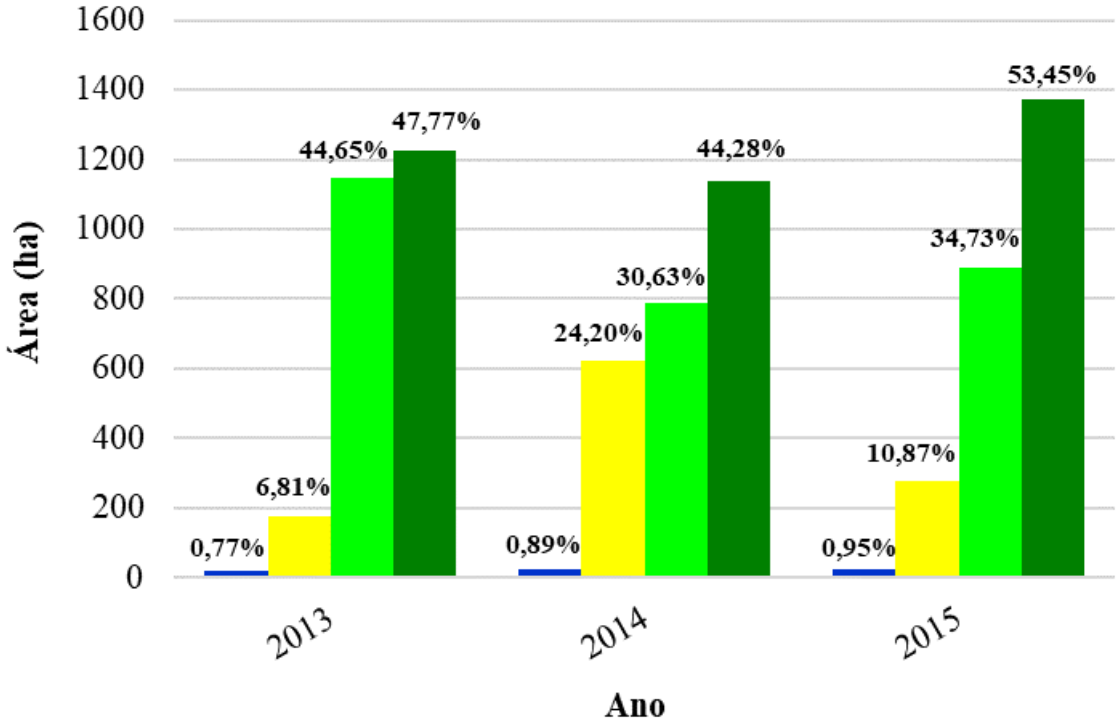

Source: Authors (2021).

Finally, through the supervised classification method maximum likelihood, it was possible to observe that the sugarcane classes (initial and maturation phenological stages) were present in most of the study area, with values of approximately 1147 and 1227 ha, 786.5 and 1137 ha and 892 and 1372.5 ha, in 2013, 2014 and 2015, respectively.

5.2 Vegetation indices and temperatures of irrigated sugarcane canopies

As with vegetation in general, the spectral response of agricultural crops depends on a series of biophysical and biochemical characteristics. The same

Typically, these factors are affected by canopy architecture, leaf chemistry, agronomic parameters and local atmospheric conditions (ABDEL-RAHMAN; AHMED, 2008).

In Figures 4a, 4b and 4c, corresponding to the dates 03/09/2013, 22/09/2014 and 24/08/2015, respectively, variations in NDVI coloration and surface temperature (Ts) can be observed, associated with the corresponding values in Table 5 below, in which the lowest NDVI values are described in blue, representing areas of water bodies and/or bare soil, whereas the highest values are displayed in red and represent areas of sugarcane with high photosynthetic activity. This same color gradient (blue and red) was also adopted to represent the oscillations in Ts analyzed in this study, as shown in Figures 4d, 4e and 4f.

Figure 4. Variability of biophysical parameters and graphical comparison of the normalized difference vegetation index (NDVI) and surface temperature (Ts) (K) in Juazeiro, BA, on 09/03/2013, 09/22/2014 and 08/24/2015.

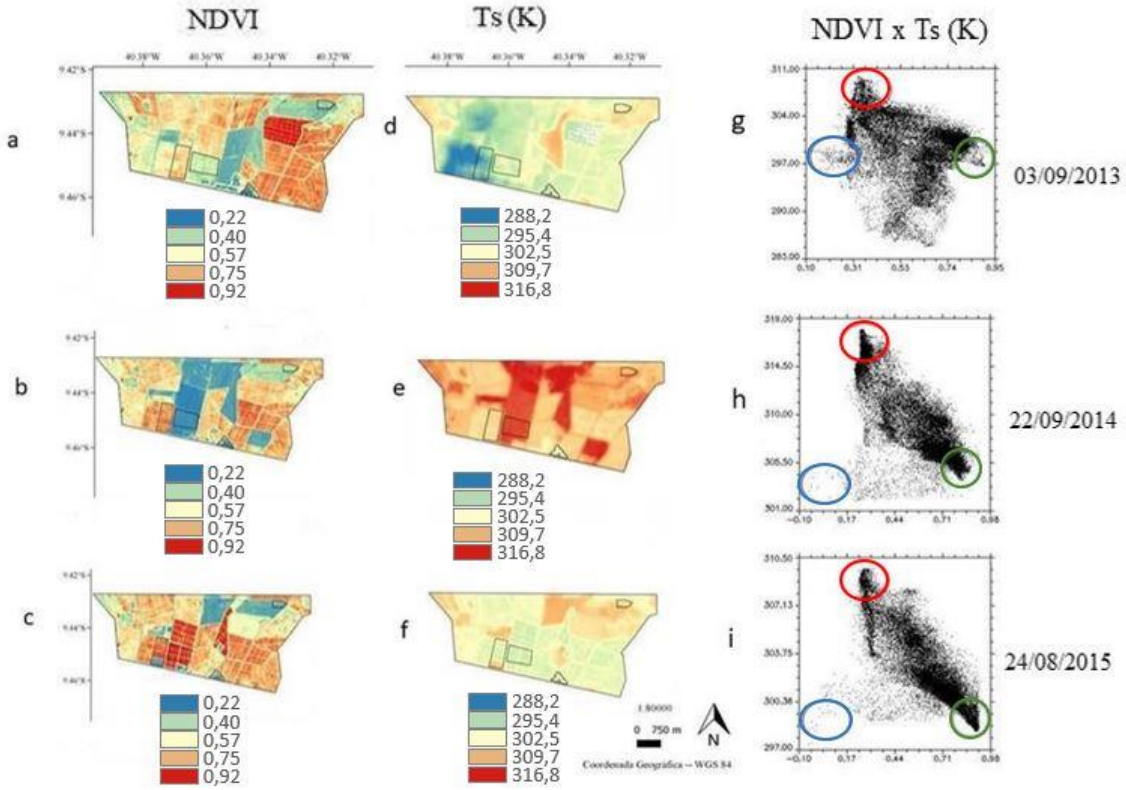

Source: Authors (2021).

Table 5. Statistical values of the biophysical parameters NDVI and Ts through Landsat-8 images in different use classes and periods in Juazeiro, BA,

Date	Parameters Biophysicists	Land Use and Occupation Classes			
		Initial Internship	Maturation	Bare Ground	Water
09/03/2013	NDVI	0.27 - 0.40	0.49 - 0.73	0.23 - 0.36	0.03 - 0.11
	Ts (K)	303 - 305	287 - 298	299- 309	293 - 300
September 22, 2014	NDVI	0.36 - 0.42	0.63 - 0.84	0.20 - 0.33	0.01 - 0.13
	Ts (K)	308 - 311	305 - 309	311 - 315	302 - 309
08/24/2015	NDVI	0.27 - 0.35	0.25 - 0.88	0.22 - 0.38	(-0.04) - 0.15
	Ts (K)	304 - 308	299 - 308	298 - 304	299 - 304
		Pixel number			
		165	658	666	183

NDVI – normalized difference vegetation index, Ts – surface temperature, K – Kelvin.
Source: Authors (2021).

Figures 4g, 4 h, and 4i present the relationships between the NDVI and Ts. The blue circles represent pixels in water bodies with low NDVI and temperature values. The red circles represent soil exposed to straw, which has low NDVI and high Ts values. Healthy vegetation (green circles) presented significant NDVI values (above 0.7) and low Ts values, close to 300 K (27 °C).

The NDVI and Ts parameters also exhibit opposite patterns; that is, the higher the NDVI is, the lower the surface temperature. Furthermore, the scatterplot

between the NDVI and Ts has a triangular shape for the different land use combinations, which is consistent with the results of Zhou *et al*. (2011). Deng *et al.* (2018) excluded water body pixels and reported that the NDVI-Ts relationship formed a right triangle, similar to the results of Price (1990).

According to Table 5, the NDVI values increased from the initial stage to the maturity stage across the three dates analyzed. This fluctuation between these land use classes results from plant emergence, which consequently gradually reduces soil exposure due to the significant increase in the plant canopy until the full crop stage, when the highest values of this index were observed (0.84 and 0.88 in 2014 and 2015, respectively) and, therefore, did not reach the maximum value of +1.

Oliveira (2017) classified NDVI values between 0.4 and 0.5 as sparse vegetation and 0.0 to 0.4 as exposed soil. Gusmão *et al.* (2013) obtained Ts values with average values lower than 294 K in water bodies. Lins *et al*. (2017), using Landsat-8 images in the semiarid region, reported that Ts presented an abrupt difference between areas with dense vegetation and those with a transition to exposed or urbanized soil, ranging from 26.45°C to 41.95°C.

Temporal analysis of the NDVI and Ts revealed variations in soil cover within a single plot, indicating differences between the phenological phases of sugarcane cultivation. An example of this is the change in the bare soil area from 2014--2015, which became irrigated sugarcane, which was also due to the decrease in surface temperature. This was also observed by Silva *et al.* (2019b), who, by maintaining soil cover with straw, reported that the air temperature changed only after canopy closure, increasing the leaf area and decreasing soil exposure. The presence of straw also contributed to an increase in soil moisture.

5.3 Albedo and net radiation of irrigated sugarcane fields

Figure 5 shows the variations in albedo color and net radiation (Rn, W/m²) of the irrigated sugarcane fields. The lowest albedo values are shown in blue, representing water bodies. The highest values, shown in red, highlight high photosynthetic activity. In the Rn figures, the red colors represent high Rn values associated with water bodies, whereas the other colors represent the lowest Rn values associated with vegetation or bare soil.

Figure 5. Variability in the biophysical parameters and linear relationships between albedo and radiation balance (Rn) (W m $^{-2}$) in Juazeiro, BA, on 09/03/2013, 09/22/2014 and 08/24/2015.

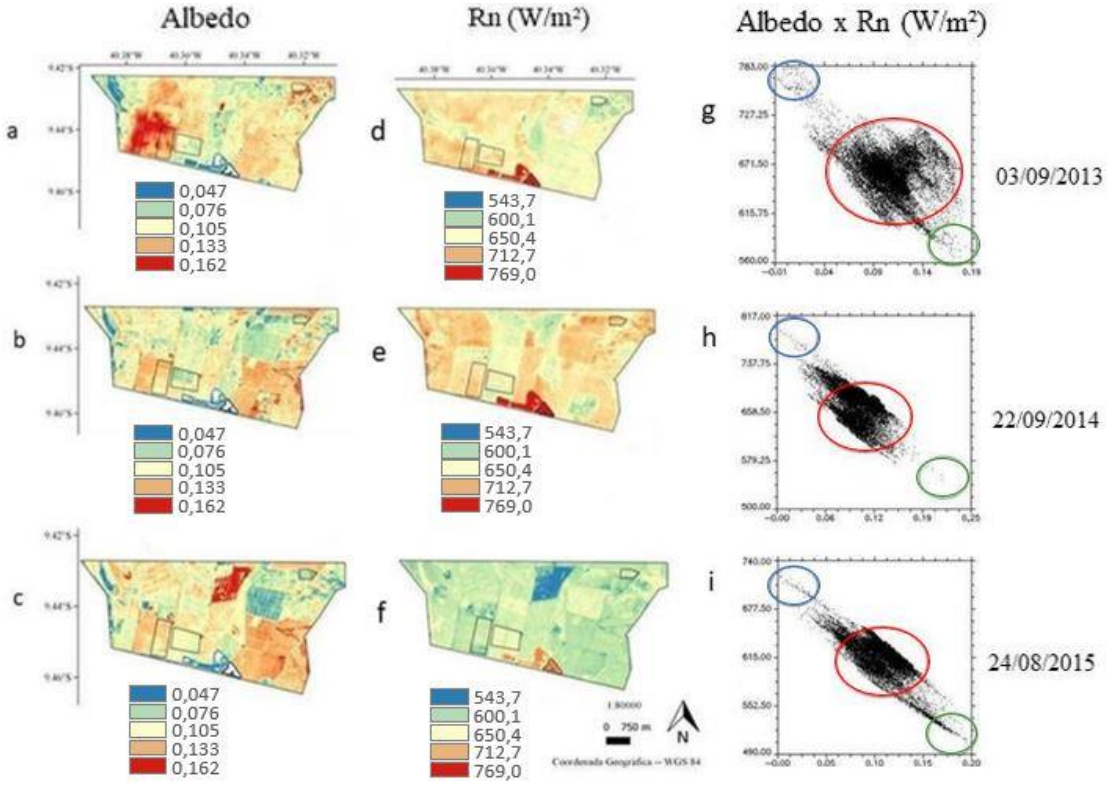

Source: Authors (2021).

The surface albedo (Figures 5a, 5b and 5c) ranged between 0.047 and 0.076 in water and between 0.08 and 0.10 in soil exposed to straw; however, in the sugarcane region in the initial stage, it was between 0.10 and 0.13, and in developing or maturing sugarcane, it was between 0.13 and 0.16, as shown in Table 6.

Table 6. Statistical values of biophysical parameters for albedo and Rn through Landsat-8 images in different use classes and periods in Juazeiro, BA.

Date	Parameters	Land Use and Occupation Classes			
	Biophysicists	Initial Internship	Maturation	Bare Ground	Water
09/03/2013	Albedo	0.08 - 0.10	0.11 - 0.16	0.07 - 0.13	0 - 0.04
	Rn (W m $^{-2}$)	600 - 656	628 - 711	648 - 707	720 - 769
September	Albedo	0.06 - 0.90	0.10 - 0.14	0.07 - 0.12	0 - 0.03
22, 2014	Rn (W m $^{-2}$)	660 - 721	655 - 701	616 - 683	747 - 768
	Albedo	0.06 - 0.10	0.08 - 0.14	0.08 - 0.13	0 - 0.03
08/24/2015	Rn (W m $^{-2}$)	590 - 647	575 - 640	596 - 656	688 - 730
		Pixel number			
		165	658	666	183

Rn – Radiation balance.
Source: Authors (2021).

The results described in Table 6 are in agreement with those reported by Mendonça *et al*. (2013), who obtained average albedo values in sugarcane between 0.12 and 0.24, also corroborated the values of bare soil, with Bastiaanssen (1995), who reported values between 0.08 and 0.14 in bare soil with dark coloration and 0.15 to 0.25 in pasture or lawn cover. Albedo values close to zero are associated with surface water from the irrigation system used.

However, Silva *et al*. (2011) reported that the dry period contributes significantly to increasing albedo values, as do areas with low water availability, thus reinforcing the findings of the study by Silva *et al*. (2019a) in the northeastern semiarid region of Brazil, in which the authors reported relatively high albedo values in years classified climatically as dry due to low rainfall and consequently prolonged drought in the region.

Rn (Figures 5e, 5f, and 5 g) presented higher values in water bodies (ranging from 712 to 769 W m $^{-2}$) and in sugarcane area 2 (ranging between 600 and 712 W m $^{-2}$); that is, the greater amount of energy available in these two areas can be used in the processes of soil evaporation and transpiration. Notably, this phenomenon was reported by Fernandes *et al*. (2019) reported that the largest fractions of Rn were associated with latent and sensible heat; however, their dynamics are likely controlled by water availability.

According to Bastiaanssen (1995), typical Rn values should be in the range of 100--700 W m $^{-2}$, depending on the surface. Mendonça *et al*. (2013) reported Rn values in sugarcane areas between 332 W m $^{-2}$ and 670 W m $^{-2}$. Notably, on September 3, 2013, the presence of clouds in the area increased albedo values, thus reducing Rn values.

As shown in Figures 5g, 5 h and 5i, there is an inverse linear relationship between albedo and Rn. In water bodies (blue circles), the albedo was low at the same time that Rn was high, consequently favoring evaporation, whereas in areas with exposed soil with straw (red circles), the albedo was relatively high, allocating most of Rn to heating the air and soil and evaporating.

Healthy sugarcane canopies (green circles) at different phenological stages presented high albedo indices and reduced Rn values due to the distribution of energy available for the processes of photosynthesis, evapotranspiration, heating of the canopy and the air above the canopy, similar to what was observed by Carvalho, Moura and Silva (2018), who reported that the change in microclimate resulting from the presence of straw modified the speed of sugarcane leaf emergence with very little effect on the efficiency of the crop's radiation balance.

Carvalho, Moura, and Silva (2018), when evaluating the behavior of radiation and energy flux in the semiarid Northeast China, reported high albedo values in areas cultivated with sugarcane compared with the native vegetation of the Caatinga, which stood out because of the emission of surface longwave radiation. This difference in radiation balance can be directly influenced at a given time of year by soil moisture from irrigated areas or rainfall, in addition to the crop's plant biomass or significant native vegetation.

Lopes *et al* . (2013) reported that the availability of energy flow in pastures was lower, significantly contributing to these areas becoming hotter compared with their adjacent neighborhood, corroborating the distribution of energy flow in the native vegetation of the Caatinga, where 64% of the radiation balance was allocated to heating the air, whereas in areas cultivated with sugarcane, 85% of the Rn contributed to the evapotranspiration process (CARVALHO; MOURA; SILVA, 2018), behavior observed in Figures 5g, 5 h and 5i.

6 CONCLUSIONS

- The methodology proved to be viable for mapping biophysical variables on different imaging dates from the Landsat-8 satellite;
- The biophysical parameters showed spatial and temporal variability, even in a small test area, due to the great heterogeneity of land use and cover;
- The sugarcane area with more developed vegetative vigor needed, on average, more available energy flow to carry out the evaporation and transpiration processes;
- In general, the reduced values presented by the NDVI were associated with high Ts and albedo with low Rn, which are directly related to exposed soil, sugarcane straw and a low presence of moisture;
- In healthy vegetation, the NDVI was high due to the significant photosynthetic activity present, with conditionally low Ts and relatively moderate albedo and Rn.

7 REFERENCES

ABDEL-RAHMAN, E.; AHMED, FB The application of remote sensing techniques to sugarcane (Saccharum spp. hybrid) production: a review of the literature. **International Journal of Remote Sensing** , Bristol, vol. 29, no. 13, p. 3753-3767, 10 July. 2008. DOI: https://doi.org/10.1080/01431160701874603. Available at: https://www.tandfonline.com/tres20. Accessed on: February 20, 2021.

ALLEN, RG; TASUMI, M.; TREZZA, R. **SEBAL -** Surface Energy Balance Algorithms for Land. Advanced training and user's manual. Version 1.0. Moscow: Idaho Implementation, 2002. Available at: http://www.posmet.ufv.br/wp-content/uploads/2016/09/MET-479-Waters-et-al-SEBAL.pdf. Accessed on: March 22, 2020.

ALVES, LER; GOMES, HB; SANTOS, MN; FREITAS, IGF Radiation balance through the Landsat-8 satellite in the Pajeú River basin. **Journal of the Department of Geography** , São Paulo, v. 33, n. 1, p. 117-127, 2017. DOI: https://doi.org/10.11606/rdg.v33i0.124577. Available at: https://www.revistas.usp.br/rdg/article/view/124577. Accessed on March 13, 2021.

ANDRADE, RG; SEDIYAMA, G.; SOARES, VP; GLERIANI, JM; MENEZES, SJMC Sugarcane productivity estimation using SEBAL and Landsat images. **Brazilian Journal of Meteorology** , São José dos Campos, v. 29, n. 3, p. 433-442, 2014. DOI: http://dx.doi.org/10.1590/0102-778620130022. Available at: https://www.scielo.br/j/rbmet/a/jJVB4 mM3ShwP6QWy49NW4pw/?format=pdf&lang=pt Accessed on: March 22, 2021.

ANDRÉ, RGB; MENDONÇA, JC; MARQUES, VS; PINHEIRO, FMA; MARQUES, J. Energy aspects of sugarcane development. Part 1: radiation balance and derived parameters. **Brazilian Journal of Meteorology** , São José dos Campos, v. 25, n. 3, p. 375-382, 2010. DOI: https://doi.org/10.1590/S0102-77862010000300009. Available at: https://www.scielo.br/j/rbmet/a/3f9pF75h5Sz5wL6QBZptsyN/Accessed on: Apr 21, 2021.

BARBOSA, HA; HUETE, AR; BAETHGEN, W.E. A 20-year study of NDVI variability over the northeast region of Brazil. **Journal of arid environments** , London, v. 67, n. 2, p. 288-307, 2006. DOI: https://doi.org/10.1016/j.jaridenv.2006.02.022. Available at: https://pubmed.ncbi.nlm.nih.gov/27077114. Accessed on: April 20, 2021.

BASTIAANSSEN, WGM Regionalization of surface flux densities and moisture indicators in composite terrain: A remote sensing approach under clear skies in Mediterranean climates. 1995. Thesis (Doctorate in Philosophy) - Wageningen Agricultural University, Wageningen, 1995.

BASTIAANSSEN, WGM SEBAL – Based sensitive and latent heat fluxes in the irrigated gediz basin, Turkey. **Journal of Hydrology** , Amsterdam, v. 229, no. 1-2, p. 87-100, 2000. DOI: https://doi.org/10.1016/S0022-1694(99)00202-4. Available at: https://www.sciencedirect.com/science/article/abs/pii/S0022169499002024. Accessed on: May 2, 2021.

BASTIAANSSEN, WGM; MENENTI, M.; FEDDES, RA; HOLTSLAG, AAM A remote sensing surface energy balance algorithm for land (SEBAL) 2. Validation. **Journal of Hydrology** , Amsterdam, v. 212-213, n. 1, p. 213-229, 1998a. DOI: https://doi.org/10.1016/S0022-1694(98)00254-6. Available at: https://www.sciencedirect.com/science/article/abs/pii/S0022169498002546?via%3Dihub. Accessed on: May 15, 2021.

BASTIAANSSEN, WGM; NOORDMAN, EJM; PELGRUM, H.; DAVIDS, G.; THORESON, BP; ALLEN, RG SEBAL model with remotely sensed data to improve water resources management under current field conditions. **Journal of Irrigation and Drainage Engineering** , New York , vol. 131, n.1, p. 85-93, 2005. DOI: h ttp://dx.doi.org/10.1061/(ASCE)0733-9437(2005)131:1(85). Available at: https://ascelibrary.org/doi/10.1061/%28ASCE%290733-9437%282005%29131%3A1%2885%29. Accessed on: 15 Feb. 2021

BASTIAANSSEN, WGM; PELGRUM, H.; WANG, J.; MA, Y.; MORENO, JF; ROERINK, GJ; VAN DER WAL, T. A remote sensing surface energy balance algorithm for land (SEBAL) 1. Formulation. **Journal of Hydrology** , Amsterdam, v. 212-213, n. 1, p. 198-212, 1998b. DOI: https://doi.org/10.1016/S0022-1694(98)00253-4 . Available at: https://www.sciencedirect.com/science/article/abs/pii/S0022169498002534 . Accessed on: February 15, 2021

SUGARCANE. Monitoring the Brazilian sugarcane harvest, Brasília, v. 6, n. 4, p. 1-58, 2020. 2019/20 Harvest, Fourth Survey. Available at: https://www.conab.gov.br/info-agro/safras/cana/boletim-da-safra-de-cana-de-acucar/item/download/31590_6cfbbc41aa04783c69113c50fa499cba. Accessed on: February 24, 2021.

CARVALHO, HFS; MOURA, MSB; SILVA, TGF Radiation and energy fluxes in preserved caatinga and sugarcane in semiarid. **Brazilian Journal of Meteorology** , São José dos Campos, v. 33, n. 3, p. 452-458, 2018. DOI: https://doi.org/10.1590/0102-7786333005. Available at:

https://www.scielo.br/j/rbmet/a/xXL9jLYNRTCLYmcDWGTH9sh/abstract/?lang=pt. Accessed on: June 24, 2021.

CECHIM J, C.; JOHANN, JA; ANTUNES, JFG Mapping of sugarcane cultivated area in the state of Paraná with Landsat/TM/OLI and IRS/LISS-3 images. **Brazilian Journal of Agricultural and Environmental Engineering** , Campina Grande, v. 21, n. 6, p. 427-432, 2017. DOI: DOI: http://dx.doi.org/10.1590/1807-1929/agriambi.v21n6p427-432. Available at: https://www.scielo.br/j/rbeaa/a/YfCJzrj4GcqhWDCWBpQ9HGF/?format=pdf. Accessed on: May 24, 2021.

CHAVEZ, JL; GOWDA, PH; HOWELL, TA; GARCIA, LA; COPELAND, KS; NEALE, CMU ET mapping with high resolution airborne remote sensing data in an advective semiarid environment. **Journal of Irrigation and Drainage Engineering,** New York , v. 138, n. 5, p. 416-423, 2012. DOI: http://dx.doi.org/10.1061/(ASCE)IR.1943-4774.0000417. Available at: https://ascelibrary.org/doi/10.1061/%28ASCE%29IR.1943-4774.0000417. Accessed on: May 1, 2021.

CONGEDO, L. Semi-Automatic Classification Plugin: A Python tool for the download and processing of remote sensing images in QGIS. **Journal of Open Source Software** , California, v. 6, n.64, p. 3172, 2021. DOI: https://doi.org/10.21105/joss.03172 . Available at: https://joss.theoj.org/papers/10.21105/joss.03172. Accessed on: March 1, 2021.

CRUZ, FN; BORBA, GL; ABREU, LRD **Natural sciences and reality:** interdisciplinary. Natal: EDUFRN, 2005.

DEBASTIANI, AB; SÁ, EAS; NETO, RPM; SCHIMALSKI, MB Mapping of the radiation balance in the São Joaquim National Park – SC. **Advances in Forestry Science** , Cuiabá, v. 5, n. 3, p. 363-367, 2018. DOI: https://doi.org/10.34062/afs.v5i3.5012. Available at: https://periodicoscientificos.ufmt.br/ojs/index.php/afor/article/view/5012. Accessed on: August 1, 2021.

DENG, Y.; WANG, S.; BAI, X.; TIAN, Y.; Wu, L.; XIAO, J.; CHEN, F.; QUIAN, Q. Relationship between land surface temperature and LUCC, NDVI in typical karst area. **Scientific Reports** , London, vol. 8, no. 641, p. 1-12, 2018. DOI: https://doi.org/10.1038/s41598-017-19088-x. Available at: https://www.nature.com/articles/s41598-017-19088-x.pdf. Accessed on: 02 Jul. 2021.

ESTEVES, BS; SOUSA, EF; MENDONÇA, JC; LOUSADA, LL; MUNIZ, RA Variations of albedo, NDVI and SAVI during a sugarcane cycle in Northern Fluminense . **Brazilian Journal of Agricultural Sciences** , Recife, v. 7, n. 4, p. 663-670, 2012. DOI: https://doi.org/10.5039/agraria.v7i4a1597. Available at: https://docs.academicoo.com/user/barbbarase/albedo.pdf. Accessed on: June 12, 2021.

FAUSTO, MA; ANGELINI, LP; MARQUES, HO; SILVA FILHO, A.; MACHADO, NG; BIUDES, MS Impact of land use change on the radiation balance in the cerrado of southern Mato Grosso. **Environment & Water Journal** , Taubaté, v. 11, n. 2, p. 350-361, 2016. DOI: https://doi.org/10.4136/ambi-agua.1843. Available at:

https://www.scielo.br/j/ambiagua/a/5TjnX6VQrtmBkqHTR6FQk3p/. Accessed on: April 5, 2020.

FERNANDES, GST; LOPES, PMO; MELO, CGB; LIMA, RLF; SANTOS, A.; SILVA, DAO Radiation balance in areas of agricultural expansion in southwestern Piauí. 7, n. 1, p. 13-20 , 2021a. DOI: **https://doi.org/10.21680/2447-3359.2021v7n1ID19704** . Available at: https://periodicos.ufrn.br/revistadoregne/article/view/19704. Accessed on: February 11, 2021.

FERNANDES, GST; LOPES, PMO; MOURA, GBA; SILVA, MV; GALVÍNCIO, JD; SANTOS, A. Balance of photosynthetically active radiation by remote sensing in a seasonally dry tropical forest in Northeastern Brazil. **Revista Brasileira de Geografia Física** , Recife, v. 14, n. 4, p. 2486-2509, 2021b. DOI: https://doi.org/10.26848/rbgf.v14.4.p2486-2508. Available at: https://periodicos.ufpe.br/revistas/rbgfe/article/view/251459. Accessed on: February 17, 2019.

FERNANDES, GST; LOPES, PMO; OLIVEIRA, VB; SILVA, DAO Energy balance by remote sensing in Caatinga fragments in southern Piauí. **Journal of Hyperspectral Remote Sensing** , Recife, v. 9, n. 3, p. 131-137, 2019. DOI: http://dx.doi.org/10.29150/jhrs.v9.3.p131-137. Available at: https://periodicos.ufpe.br/revistas/jhrs/article/view/242133. Accessed on: February 11, 2021.

FERREIRA JUNIOR, RA; SOUZA, JL; LYRA, GB; ESCOBEDO, JF; SANTOS, MVC Energy conversion efficiency in sugarcane under two row spacings in Northeastern Brazil. **Brazilian Journal of Agricultural and Environmental Engineering** , Campina Grande, v. 19, n. 8, p. 741-747, 2015. DOI: https://doi.org/10.1590/1807-1929/agriambi.v19n8p741-747. Available at: https://www.scielo.br/j/rbeaa/a/KKCQy59XVwyXbMb6KcgFV8K/?lang=en. Accessed on: November 21, 2020.

GUSMÃO, ACVL; SILVA, BBD; MONTENEGRO, SM; GALVÍNCIO, JD Determination of the radiative balance on Bananal Island, TO, with orbital images. **Brazilian Journal of Agricultural and Environmental Engineering** , Campina Grande, v. 16, n. 1, p. 1107-1114, 2012. DOI: https://doi.org/10.1590/S1415-43662012001000011. Available at: https://www.scielo.br/j/rbeaa/a/VrCq3k4FcYN934D8Mh6Kk4k/?lang=pt. Accessed on: December 31, 2020.

GUSMÃO, ACVL; SILVA, BB; MONTENEGRO, SMGL; GALVÍNCIO, JD; OLIVEIRA, LMM Vegetation index and surface temperature in the Bananal Island ecotone by remote sensing. **Revista de Geografia** , Recife, v. 30, n. 3, p. 209-225, 2013. Available at: https://periodicos.ufpe.br/revistas/revistageografia/article/view/229114. Accessed on: February 23, 2020. Accessed on: December 15, 2020.

HUETE, AR A soil-adjusted vegetation index (SAVI) . **Remote Sensing of Environment** , New York , v. 25, n. 3, p. 295-309, 1988. DOI: https://doi.org/10.1016/0034-4257(88)90106-X. Available at: https://www.sciencedirect.com/science/article/abs/pii/003442578890106X?via%3Dihub. Accessed on: May 15, 2020.

HUETE, A.; DIDAN, K.; MIURA, T.; RODRIGUEZ, EP; GAO, X.; FERREIRA, LG Overview of the radiometric and biophysical performance of the MODIS vegetation indices. **Remote Sensing of Environment** , New York , v. 83, n. 1-2, p. 195-213, 2002. DOI: https://doi.org/10.1016/S0034-4257(02)00096-2. Available at: https://www.sciencedirect.com/science/article/abs/pii/S0034425702000962?via%3Dihub. Accessed on: May 13, 2020.

INPE. National Institute for Space Research. Earth System Science Center. 2020. Available at: http://sonda.ccst.inpe.br/. Accessed on: January 19, 2020.

JULIEN, Y.; SOBRINO, JA The annual land cover dynamics (YLCD) method: An analysis of global vegetation from NDVI and LST parameters. **Remote Sensing of Environment** , New York , v. 113, n. 1, p. 329-334, 2009. DOI: https://doi.org/10.1016/j.rse.2008.09.016. Available at: https://www.sciencedirect.com/science/article/abs/pii/S0034425708003131?via%3Dihub. Accessed on: January 17, 2020.

LINS, FAC; ARAÚJO, DCS; SILVA, JLB; LOPES, PMO; OLIVEIRA, JDA; SILVA, ATCSG Estimation of biophysical parameters and actual evapotranspiration in the semiarid region of Pernambuco using remote sensing. **Irriga Journal** , Botucatu, v. 1, n. 1, p. 64-75, 2017. DOI: https://doi.org/10.15809/irriga.2017v1n1p64-75. Available at: https://irriga.fca.unesp.br/index.php/irriga/article/view/2801. Accessed on: March 10, 2020.

LOPES, PMO; VALERIANO, DM; SILVA, BB; MOURA, GBA; SILVA, AO Simulation of the net radiation in the Mantiqueira Mountain Range, **Brazilian Journal of Agricultural and Environmental Engineering** , Campina Grande, v. 17, n. 7, p. 780-789, 2013. DOI: https://doi.org/10.1590/S1415-43662013000700013. Available at: https://www.scielo.br/j/rbeaa/a/NnKd4yWnPbkGsnnFFMFKjJS/?lang=pt. Accessed on: January 21, 2022.

MACHADO, CC; SILVA, BB; ALBUQUERQUE, MB; GALVÍNCIO, JD Energy balance estimation using TM – Landsat 5 images and the SEBAL algorithm on the southern coast of Pernambuco. **Brazilian Journal of Meteorology** , São José dos Campos, v. 29, n. 1, p. 55-67, 2014. DOI: https://doi.org/10.1590/S0102-77862014000100006. Available at: https://www.scielo.br/j/rbmet/a/x6FXKzvfrSRhCVjk4BFZRdQ/?lang=pt. Accessed on: January 19, 2022.

MARTINS, CMR; LOPES, PMO; MOURA, GBA; SILVA, Ê. FF; NÓBREGA, RS; SILVA, JLB Evapotranspiration of sugarcane in different phenological phases by remote sensing in the São Francisco Submedium Valley. **Journal of Hyperspectral Remote Sensing** , Recife, v. 9, no. 3, p. 156-165, 2019. DOI: https://doi.org/10.29150/jhrs.v9.3.p156- 165. Available at: https://periodicos.ufpe.br/revistas/jhrs/article/view/242182. Accessed on: January 19, 2022.

MARTINS, GD; GALO, MLBT Spectral characterization of sugarcane infected by nematodes and migdolus fryanus by field spectroradiometry. **Bulletin of Geodetic Sciences** , Paraná , v. 21, n. 4, p. 783-796, 2015. DOI: http://dx.doi.org/10.1590/S1982-21702015000400046. Available at: https://www.scielo.br/j/bcg/a/r4r49y3xjmrdBZLysRZZjbm/?lang=pt. Accessed on: January 18, 2022.

MATINFAR, HR Evapotranspiration estimation base upon SEBAL model and fieldwork. **Annals of Biological Research,** Kragujevac, v. 3, n. 5, p. 2459-2463, 2012. Available at: https://www.scholarsresearchlibrary.com/articles/evapotranspiration-estimation-base-upon-sebal-model-and-fieldwork.pdf. Accessed on: January 12, 2021.

MENDONÇA, JC; SOUZA, EF; ANDRÉ, RGB; SILVA, BB; FERREIRA, NJ Crop coefficient (KC) of sugarcane in a subhumid region of Brazil, by applying the SEBAL algorithm and MODIS products. *In* : SILVA, BB **Brazilian Environmental Applications of Geoprocessing and Remote Sensing** . Campina Grande: EDUFCG, 2013. chap. 4, p. 71-86.

MULIANGA, B.; BÉGUÉ, A.; CLOUVEL, P.; TODOROFF, P. Mapping Cropping Practices of a Sugarcane-Based Cropping System in Kenya Using Remote Sensing. **Remote Sensing** , New York , v. 7, n. 11, p. 14428-14444, 2015. DOI: https://doi.org/10.3390/rs71114428. Available at: https://www.mdpi.com/2072-4292/7/11/14428. Accessed on: January 18, 2022.

NASCIMENTO, EF; PEREIRA, FAC; AGUIAR NETTO, AO; CAMPECHE, LFS M; SANTOS, CA Physical-hydric behavior of soils in the Curaçá irrigated perimeter in Juazeiro/BA. **Irriga** , Botucatu, v. 17, n. 4, p. 435-447, 2012. DOI: https://doi.org/10.15809/irriga.2012v17n4p435. Available at: https://revistas.fca.unesp.br/index.php/irriga/article/view/103. Accessed on: January 18, 2022.

NEMUS. **Water resources plan for the São Francisco River basin** . Investment Booklet for the São Francisco River basin 2016-2025. Salvador: NEMUS, 2016. Available at: https://2017.cbhsaofrancisco.org.br/wp-content/uploads/2016/08/PRH-SF_Apresentacao_26ago16.pdf . Accessed on: January 20, 2022

OLIVEIRA, G.; MORAES, EC; RUDORFF, BFT Radiation balance in sugarcane expansion areas in São Paulo state using MODIS/Aqua orbital data. **Brazilian Journal of Cartography** , Uberlândia, v. 66, n. 3, p. 419-431, 2014. Available at: http://www.seer.ufu.br/index.php/revistabrasileiracartografia/article/view/44752. Accessed on: November 18, 2019.

OLIVEIRA, JDA **Assessment of degradation and environmental changes in the upper Ipanema river basin** . 2017. Dissertation (Master's Degree in Postgraduate Program in Agricultural Engineering) – Federal Rural University of Pernambuco, Recife, 2017. Available at: http://www.tede2.ufrpe.br:8080/tede2/handle/tede2/7644. Accessed on: April 28, 2020.

OLIVEIRA, LMM; SILVA, BB; MOURA, AESS Radiation balance by remote sensing in a river basin of the northeastern forest zone. **Brazilian Journal of Meteorology** , São José dos Campos, v. 30, n. 1, p. 16-28, 2015. DOI: https://doi.org/10.1590/0102-778620130652. Available at: https://www.scielo.br/j/rbmet/a/qM3n4kVq5vg4ShxNYtmBqrz/?lang=pt. Accessed on: January 21, 2022.

OLIVEIRA, RK; FRAGA JUNIOR, LS; MOURA, LB; ROBERTI, DR; PILAU, FG Energy balance in a renewal sugarcane area with fallow period and soybean cultivation. **Ciência e Natura** , Santa Maria, RS , v. 42, p. e39, 2020. DOI:

https://doi.org/10.5902/2179460X53222. Available at: https://periodicos.ufsm.br/cienciaenatura/article/view/53222. Accessed on: January 21, 2022.

PAGANI, V.; STELLA, T.; GUARNERI, T.; FINOTTO, G.; BERG, MVD; MARIN, FR; ACUTIS, M.; CONFALONIERI, R. Forecasting sugarcane yields using agro-climatic indicators and Canegro model: A case study in the main production region in Brazil. **Agricultural Systems** , Essex, vol. 154 , p. 45-52, 2017. DOI: http://dx.doi.org/10.1016/j.agsy.2017.03.002. Available at: https://www.sciencedirect.com/science/article/abs/pii/S0308521X16308095?via%3Dihub. Accessed on: 21 Jan. 2022.

PINHEIRO, MPM A; CRUZ, RL; SIMÕES, WL Behavior of water content in a soil cultivated with sugarcane irrigated with different depths. **Brazilian Journal of Renewable Energy** , Cascavel, v. 4, n. 1, p. 30-42, 2015. Available at: https://revistas.ufpr.br/rber/article/view/40544. Accessed on: November 30, 2019.

PRICE, JC Using spatial context in satellite data to infer regional scale evapotranspiration. **IEEE Transactions on Geoscience & Remote Sensing** , New York , v. 28, no. 2, p. 940-948, 1990. DOI: https://doi.org/10.1109/36.58983 . Available at: https://ieeexplore.ieee.org/document/58983. Accessed on: November 30, 2019.

RIDESA. Interuniversity Network for the Development of the Sugarcane Sector. 2019. Available at: https://www.ridesa.com.br. Accessed on: September 24, 2020

RODRIGUES, JAM; LOPES, PMO; SILVA, JLB; ARAÚJO, HL; SILVA, MV; SANTOS, A.; MOURA, GBA Spatial-temporal dynamics of Caatinga vegetation cover by remote sensing in the Brazilian semiarid region. **Dyna** , Medellin, v. 87, no. 215, p. 109-117, 2020. DOI: https://doi.org/10.15446/dyna.v87n215.87851. Available at: https://revistas.unal.edu.co/index.php/dyna/article/view/87851. Accessed on: January 20, 2022

ROUSE, JW; HAAS, RH; SCHELL, JA; DEERING, DW; HARLAN, JC **Monitoring the vernal advancement of retrogradation of natural vegetation** . Greenbelt: Goddard Space Flight Center , 1973.

SÁ, PCC **Estimation of net radiation in irrigated sugarcane cultivation using orbital remote sensing data** . 2016. Dissertation (Master's Degree in Postgraduate Program in Soil and Water Management) – Federal Rural University of Semi-Arid, Mossoró, 2016.

SILVA, BB; BRAGA, AC; BRAGA, CC Radiation balance in the irrigated perimeter of São Gonçalo – PB using orbital images. **Caatinga Magazine** , Mossoró, v. 24, n. 3, p. 145-152, 2011. Available at: https://periodicos.ufersa.edu.br/index.php/caatinga/article/view/2282. Accessed on: August 13, 2020.

SILVA, BB; BRAGA, AC; BRAGA, CC; OLIVEIRA, LMM; GALVÍNCIO, JD; MONTENEGRO, SMGL Evapotranspiration and estimation of water consumption in irrigated perimeter of the Brazilian semiarid region by remote sensing. **Brazilian Agricultural Research** , Brasília, v. 47, n. 9, p. 1218-1226, 2012. DOI:

https://doi.org/10.1590/S0100-204X2012000900006. Available at: https://www.scielo.br/j/pab/a/fJgHJWpGk8wcvyy7Vnp4rbh/?lang=pt. Accessed on: January 19, 2022.

SILVA, BB; BRAGA, AC; BRAGA, CC; OLIVEIRA, LMM; MONTENEGRO, SMGL; BARBOSA JUNIOR, B. Procedures for calculating the albedo with OLI-Landsat 8 images: Application to the Brazilian semiarid. **Brazilian Journal of Agricultural and Environmental Engineering** , Santa Maria, v. 20, n. 1, p. 3-8, 2016. DOI: https://doi.org/10.1590/1807-1929/agriambi.v20n1p3-8. Available at: https://www.scielo.br/j/rbeaa/a/sX6cJjNXWMfHQ5p4h33B8Zz/?lang=en. Accessed on: January 19, 2022.

SILVA, BB; LOPES, GM; AZEVEDO, PV Radiation balance in irrigated areas using Landsat 5 – TM images . **Brazilian Journal of Meteorology** , São José dos Campos, v. 20, n. 2, p. 243-252, 2005b. Available at: http://dca.ufcg.edu.br/DCA_download/ISR/UFPE/56-2004_BBarbosa-aceito.pdf. Accessed on: October 2, 2020.

SILVA, BB; LOPES, GM; AZEVEDO, PV Determination of the albedo of irrigated areas based on Landsat 5 TM images. **Brazilian Journal of Agrometeorology** , Santa Maria, v. 13, n. 2, p. 11-21, 2005a.

SILVA, BB; MONTENEGRO, SMGL; SILVA, VPR; ROCHA, HR; GALVÍNCIO, JD; OLIVEIRA, LMM Determination of instantaneous and daily net radiation from TM – Landsat 5 data in a subtropical watershed. **Journal of Atmospheric and Solar-Terrestrial Physics,** Amsterdam, v. 135, p. 42-49, 2015. DOI: http://dx.doi.org/10.1016/j.jastp.2015.09.020. Available at: https://www.sciencedirect.com/science/article/abs/pii/S1364682615300614?via%3Dihub. Accessed on: January 17, 2022.

SILVA, CVS; SILVA, JLB; MOURA, GBA; LOPES, PMO; NASCIMENTO, CR; SILVA, LC Remote sensing vegetation cover monitoring in the Brazilian semiarid region using vegetation indices. **Revista Nativa** , Sinop, v. 7, n. 6, p. 708-717, 2019a. DOI: http://dx.doi.org/10.31413/nativa.v7i6.7646. Available at: https://periodicoscientificos.ufmt.br/ojs/index.php/nativa/article/view/7646. Accessed on: January 17, 2022.

SILVA, DC; LOPES, PMO; SILVA, MV; MOURA, GBA; NASCIMENTO, CR; BRITO, JIB; FRANÇA E SILVA, EF; ROLIM, MM; LIMA, RP Principal component analysis and biophysical parameters in the assessment of soil salinity in the irrigated perimeter of Bahia, Brazil, **Journal of South American Earth Sciences** , Oxford, v. 112, Part 1, p. 103580, 2021b. DOI: https://doi.org/10.1016/j.jsames.2021.103580. Available at: https://www.sciencedirect.com/science/article/abs/pii/S0895981121004260?via%3Dihub. Accessed on: January 22, 2022.

SILVA, JC A; BACANI, V. M; CARVALHO, LA Digital image processing routines of Landsat 5/TM for the identification of fires in sugarcane fields. **Bioscience Journal** , Uberlândia, v. 29, supplement 1, p. 1514-1523, 2013. Available at:

https://seer.ufu.br/index.php/biosciencejournal/article/view/15068. Accessed on: April 22, 2021.

SILVA, JLB; MOURA, GBA; LOPES, PMO; FRANÇA E SILVA, Ê. F.; ORTIZ, PFS; SILVA, DAO; SILVA, MV; GUEDES, RVS Spatial-Temporal Monitoring of the Risk of Environmental Degradation and Desertification by Remote Sensing in a Brazilian Semiarid Region. **Revista Brasileira de Geografia Física** , Recife, v. 13, n. 2, p. 544-563, 2020. DOI: https://doi.org/10.26848/rbgf.v13.2.p544-563. Available at: https://periodicos.ufpe.br/revistas/rbgfe/article/view/242500. Accessed on: January 22, 2022.

SILVA, LC; SILVA, JLB; MOURA, GBA; SILVA, DAO; LOPES, PMO; NASCIMENTO, CR; SILVA, MV; BATISTA, PHD Biophysical indices and surface radiation balance via remote sensing in the semiarid region of Pernambuco. **Journal of Environmental Analysis and Progress** , Recife, v. 6, n. 1, p. 12-23, 2021a. DOI: https://doi.org/10.24221/jeap.6.1.2021.2876.012-023. Available at: http://www.journals.ufrpe.br/index.php/JEAP/article/view/2876. Accessed on: January 22, 2022.

SILVA, LJ **Varietal Census** - 2018/2019 harvest. Recife: Ridesa Brasil, 2019. Available at: http://www.prppg.ufrpe.br/eecac/sites/prppg.ufrpe.br.eecac/files/CENSO%20VARIETAL.pd. Accessed on: February 17, 2020.

SILVA, KJC; LOPES, PMO Spatiotemporal variation of the vegetation index by normalized difference in the hydrographic basin of Pernambuco semiarid, Brazil. **Journal of Hyperspectral Remote Sensing** , Recife, v. 11, p.292-301, 2021. DOI: https://doi.org/10.29150/jhrs.v11.5.p292-301. Available at: https://periodicos.ufpe.br/revistas/jhrs/article/view/251965. Accessed on: January 22, 2022.

SILVA, TGF; SOUZA, CAA; MOURA, MSB; MARIN, FR; CARVALHO, HFS; LEITÃO, MMVBR; GALVÍNCIO, JD Energy balance, leaf emission and radiation use efficiency of sugarcane in cultivation with and without straw. **Brazilian Journal of Meteorology** , São José dos Campos, v. 34, n. 1, p. 69-78, 2019b. DOI: http://dx.doi.org/10.1590/0102-7786334016. Available at: https://www.scielo.br/j/rbmet/a/xL8h8WZPBhPkBMdL7Ld4q8K/?lang=pt. Accessed on: January 22, 2022.

SUN, G.; ALSTAD, K.; CHEN, J.; CHEN, S.; FORD, C.R.; LIN, G.; LIU, C.; LU, N.; MCNULTY, SG; MIAO, H.; NOORMETS, A.; VOSE, J.M.; WILSKE, B.; ZEPPEL, M.; ZHANG, Y.; ZHANG, Z. A general predictive model for estimating monthly ecosystem evapotranspiration. **Ecohydrology** , Warszawa, v. 4, n. 2, p. 245-255, 2010. DOI: https://doi.org/10.1002/eco.194. Available at: https://onlinelibrary.wiley.com/doi/10.1002/eco.194. Accessed on: January 21, 2022.

TANG, R.; LI, ZL; CHEN, KS; JIA, Y.; LI, C.; SUN, X. Spatial-scale effect on the SEBAL model for evapotranspiration estimation using remote sensing data. **Agricultural and Forest Meteorology** , Amsterdam, v. 174-175, p. 28-42, 2013. DOI: https://doi.org/10.1016/j.agrformet.2013.01.008. Available at:

https://www.sciencedirect.com/science/article/abs/pii/S0168192313000130?via%3Dihub. Accessed on: January 19, 2022.

TEIXEIRA, AHC; BASTIAANSSEN, WGM; AHMAD, MD; BOS, MG Reviewing SEBAL input parameters for assessing evapotranspiration and water productivity for the Lower-Middle São Francisco River basin, Brazil Part A: Calibration and validation. **Agricultural and Forest Meteorology** , Amsterdam, v. 149, n . 462-476, 2009. DOI: https://doi.org/10.1016/j.agrformet.2008.09.016 . Available at: https://www.sciencedirect.com/science/article/abs/pii/S0168192308002566?via%3Dihub. Accessed on: January 19, 2022.

USGS. UNITED STATES GEOLOGICAL SURVEY. EarthExplorer. 2021. Available at: https://earthexplorer.usgs.gov/. Accessed on: February 20, 2021.

VIANELLO, RL; ALVES, AR **Basic meteorology and applications** . Viçosa, MG: UFV, 2012.

VON RANDOW, C.; MANZI, A.; KRUIJT, B.; DE OLIVEIRA, PJ; ZANCHI, FB; SILVA, RL; HODNETT, MG; GASH, JHC; ELBERS, JA; WATERLOO, MJ; CARDOSO, FL; KABAT, P. Comparative measurements and seasonal variations in energy and carbon exchange over forest and pasture in South West Amazonia. **Theoretical and Applied Climatology** , New York, v.78, p. 5–26, 2004. DOI: https://doi.org/10.1007/s00704-004-0041-z. Available at: https://link.springer.com/article/10.1007/s00704-004-0041-z. Accessed on: 21 Jan. 2022.

WANG, S.; GRANT, RF; VERSEGHY, DL; BLACK, TA Modeling plant carbon and nitrogen dynamics of a boreal aspen forest in CLASS - the Canadian Land Surface Scheme. **Ecology Modeling** , Amsterdam, v. 142, no. 1-2, p. 135-154, 2001. DOI: https://doi.org/10.1016/S0304-3800(01)00284-8. Available at: https://www.sciencedirect.com/science/article/abs/pii/S0304380001002848?via%3Dihub. Accessed on: 21 Jan. 2022.

WENG, Q.; LU, D.; SCHUBRING, J. Estimation of land surface temperature– vegetation abundance relationship for urban heat island studies. **Remote Sensing of Environment** , New York, v. 89, no. 4, p. 467-483, 2004. DOI: https://doi.org/10.1016/j.rse.2003.11.005. Available at: https://www.sciencedirect.com/science/article/abs/pii/S0034425703003390?via%3Dihub. Accessed on: 21 Jan. 2022.

WENG, Q.; QUATTROCHI, DA Thermal remote sensing of urban areas: An introduction to the special issue. **Remote Sensing of Environment** , New York , v. 104, n. 2, p. 119-122, 2006. DOI: https://doi.org/10.1016/j.rse.2006.05.002. Available at: https://www.sciencedirect.com/science/article/abs/pii/S0034425706001763?via%3Dihub. Accessed on: January 21, 2022.

ZHOU, Y.; SHI, TM; HU, YM; GAO, C.; LIU, M. Relationships between land surface temperature and normalized difference vegetation index based on urban land use type. **Chinese Journal of Ecology,** Shenyang, v. 30, n. 1, p. 1504-1512, 2011. Available at:

https://en.cnki.com.cn/Article_en/CJFDTotal-STXZ201107035.htm. Accessed on: January 21, 2022.